Antarctic ozone enhancement during the 2019 sudden stratospheric warming event

Sarah Safieddine, Marie Bouillon, Ana Claudia Parracho, Julien Jumelet, Florent Tencé, Andrea Pazmino, Florence Goutail, Catherine Wespes, Slimane Bekki, Anne Boynard, et al.

Geophysical Research Letters

RESEARCH LETTER
10.1029/2020GL087810

Antarctic Ozone Enhancement During the 2019 Sudden Stratospheric Warming Event

Sarah Safieddine[1], Marie Bouillon[1], Ana-Claudia Paracho[1], Julien Jumelet[1], Florent Tencé[1], Andrea Pazmino[1], Florence Goutail[1], Catherine Wespes[2], Slimane Bekki[1], Anne Boynard[1,3], Juliette Hadji-Lazaro[1], Pierre-François Coheur[2], Daniel Hurtmans[2], and Cathy Clerbaux[1,2]

[1]LATMOS/IPSL, Sorbonne Université, UVSQ, CNRS, Paris, France, [2]Université libre de Bruxelles (ULB), Laboratory of Spectroscopy, Quantum Chemistry and Atmospheric Remote Sensing (SQUARES), Brussels, Belgium, [3]SPASCIA, Ramonville-Saint-Agne, France

Abstract We analyze the 2019 sudden stratospheric warming event that occurred in the Southern Hemisphere through its impact on the Antarctic ozone. Using temperature, ozone, and nitric acid data from the Infrared Atmospheric Sounding Interferometer (IASI), our results show that the average increase in stratospheric temperature reached a maximum of 34.4° on 20 September in the [60–90]°S latitude range when compared to the past 3 years. Dynamical parameters suggest a locally reversed and weakened zonal winds and a shift in the location of the polar jet vortex. This led to air masses mixing, to a reduced polar stratospheric clouds formation detected at a ground station, and as such to lower ozone and nitric acid depletion. 2019 total ozone columns for the months of September, October, and November were on average higher by 29%, 28%, and 26%, respectively, when compared to the 11-year average of the same months.

Plain Language Summary In August and September 2019 exceptional meteorology led to a sudden increase in temperatures at altitudes between 20 and 30 km above the ground over Antarctica. This is a rare and very important event since it has direct effects on the ozone hole size and distribution. In this work, we investigate this event, using satellite and ground-based station data. We document the warming, its starting date (end of August), and how long it lasted (around 3 weeks). This warming helped in stopping the formation of high altitude icy clouds that usually trap ozone depleting species. When springtime starts (September/October), these depleting species are usually released and ozone destruction starts. This year however, and due to the warming, very little ozone destruction took place, leading to high ozone columns (small ozone hole) over Antarctica.

Key Points:
- 2019 exceptional meteorology led to sudden increase in stratospheric temperatures in Antarctica
- SSW led to high ozone and nitric acid total columns
- IASI is able to detect, measure, and follow the evolution and intensity of SSW events

Supporting Information:
- Supporting Information S1

Correspondence to:
S. Safieddine,
sarah.safieddine@latmos.ipsl.fr

Citation:
Safieddine, S., Bouillon, M., Paracho, A.-C., Jumelet, J., Tencé, F., Pazmino, A., et al. (2020). Antarctic ozone enhancement during the 2019 sudden stratospheric warming event. *Geophysical Research Letters*, *47*, e2020GL087810. https://doi.org/10.1029/2020GL087810

Received 6 MAR 2020
Accepted 11 JUN 2020
Accepted article online 23 JUN 2020

1. Introduction

Sudden stratospheric warming (SSW) events are commonly defined by the reversal or weakening of stratospheric zonal winds around the polar vortex during winter at 10 hPa and 60°, associated with a reversal of the temperature gradient poleward from 60° at 10 hPa (Andrews et al., 1987; Scherhag, 1952; WMO, 1978). SSW events are driven by dynamics where large-scale topography such as mountains, or the contrast between warm ocean temperatures and cold land masses, generate large-scale planetary waves that can propagate to the stratosphere. The breaking of these waves in the stratosphere leads to perturbation and deceleration of the polar vortex circulation, resulting in a sharp increase in temperature in the polar stratosphere (Butler et al., 2015, and references therein). The vortex initially forms because of the large meridional temperature gradient near the polar terminator during winter (Solomon, 1999). Since the northern polar vortex is generally more disturbed by planetary waves generated by the variable surface topography existing in the Northern Hemisphere (NH), SSW occur frequently in the NH every second year on average (e.g., Blume et al., 2012; Charlton & Polvani, 2007; Wang et al., 2019, among others). Examples of documented SSW events in the Southern Hemisphere (SH) are the 2002 event (Krüger et al., 2005; Varotsos, 2003; WMO, 2002) and the 2010 SSW event (de Laat & van Weele, 2011; Eswaraiah et al., 2018).

As such, SSW events lead to greater mixing at the edge of the polar vortex. This is important because strong ozone depletion occurs within the polar vortex and is directly dependent on the permeability and stability of the polar vortex (Holton et al., 1995). Polar ozone depletion is also strongly correlated with the temperature:

Springtime halogen-driven ozone depletion takes place after polar stratospheric clouds (PSCs) convert halogen reservoir species into ozone-destroying reactive forms (Solomon, 1999; Solomon et al., 1986). The sharp warming of the polar stratosphere during SSW events leads to the evaporation of PSCs and hence to the end of halogen activation.

SSW events have been shown to increase the wintertime Arctic ozone concentrations since ozone loss depends on the intensity and timing of the SSW event (Kuttippurath & Nikulin, 2012). SSW events also favor faster downward motion, by bringing down ozone-rich air from above and outside the vortex and hence strongly influence polar stratospheric ozone depletion (Solomon, 1999).

SSW events in the NH or SH lead to circulation anomalies that can propagate downward into the troposphere and impact tropospheric circulation and weather at the surface (Baldwin & Dunkerton, 1999; Baldwin, 2003; Cohen et al., 2007; Kidston et al., 2015; Lim et al., 2018, 2020). As in the NH, a SSW event in the SH occurring late winter or early spring has a direct effect on the ozone hole characteristics, for example, size, location, and duration.

In this study, we investigate the rare SSW event that started in August 2019 in the SH, forecasted to be on a par with the last large event, in 2002 (Hendon et al., 2019), which involved an exceptionally strong stationary planetary wave (Yamazaki et al., 2020). We discuss this event from an observational perspective and its effect on the ozone total columns, using ground-based measurements of temperature and PSC occurrences along with satellite measurements of temperature, ozone, and nitric acid. The paper is arranged as follows: Methods and data are briefly explained in section 2. Results are presented and discussed in section 3. We show temperature data from IASI and ground-based radio-sounding measurements; we use dynamical parameters from MERRA-2, as well as PSC lidar measurements to help in characterizing this event and explain the effect on the total columns of ozone and nitric acid. Conclusions are summarized in section 4.

2. Data Used to Study This Event

2.1. IASI Satellite Data: Temperature, Ozone, and Nitric Acid

The Infrared Atmospheric Sounding Interferometer (IASI) is a nadir-viewing spectrometer (Clerbaux et al., 2009) that has been flying on board the EUMETSAT's (European Organization for the Exploitation of Meteorological Satellites) Metop-A, Metop-B, and Metop-C satellites, since October 2006, September 2012, and November 2018, respectively.

IASI temperature profiles used in this work are disseminated by EUMETSAT (Klaes et al., 2007). The temperature product is derived mainly from IASI upwelling radiances. This data set is not homogeneous in time for Level 2 (L2) operational products (e.g., temperature, humidity, and cloud cover), as changes occurred with evolving versions of the processing algorithm (EUMETSAT, IASI Level 2, 2017), from 2008 (v4.2) to 2016 (v6.2) (Van Damme et al., 2017). The algorithm is mostly unchanged after 2016. Reprocessing the data with the latest algorithm is foreseen in a near future. In this work, and for consistency, we use temperature data from Metop-A and Metop-B, from 2016 onward. The maximum number of independent pieces of information determined in the temperature profile is around 14 (EUMETSAT, IASI Level 2, 2017). These are used as input in the radiative transfer code RTTOV and delivered to users on a 101-pressure level grid.

Retrievals for ozone (O_3) and nitric acid (HNO_3) are respectively performed in the 1,025–1,075 cm^{-1} and the 860–900 cm^{-1} of spectral ranges and rely on the optimal estimation method (Rodgers, 2000). We use a dedicated retrieval algorithm, the Fast Optimal Retrievals on Layers for IASI (FORLI-O3 and FORLI-HNO3, version 20151001) software (Hurtmans et al., 2012). Information on the algorithm, the retrieval errors, and the validation of the IASI ozone product at different altitudes and columns can be found in Hurtmans et al. (2012) and Boynard et al. (2018) and in Ronsmans et al. (2016) for HNO_3. IASI-A and IASI-B ozone data are in agreement with differences in the Antarctic region during the study period that are less than 1% for O_3 and 7.5% for HNO_3 (higher inversion errors for HNO_3), and therefore, we choose to combine the IASI-A and IASI-B products in this work. Moreover, Boynard et al. (2018) showed that the IASI-A total ozone column product has no significant drift during the 2008–2017 record. The validation of FORLI-HNO_3 with FTIR measurements also showed similar conclusive results (Ronsmans et al., 2016). Operational data from Metop-C start on 20 September 2019 and are not included in this work since the SSW event analyzed here starts earlier.

2.2. Dumont d'Urville Ground-Based Measurements: Temperature, O_3, and PSC Monitoring

In the framework of the Network for the Detection of Atmospheric Composition Change (NDACC), measurements are carried out at the French Antarctic station Dumont d'Urville (DDU) (66°S to 140°E) since 1989 with logistic support by the French Polar institute. Lidar measurements are performed at nighttime from around March to October, to monitor the occurrences and optical properties of aerosol layers, tropopause cirrus, and PSC (David et al., 1998, 2012). The lidar is a Rayleigh/Mie/Raman instrument emitting at 532 nm with orthogonal polarization retrieving light backscattered from the effective [6–40] km altitude range. In this study, we use the 532-nm attenuated backscatter as cloud presence indicator. The instrumental vertical resolution is 60 m, and time resolution is 3 min. Those individual files are summed according to the dynamics of the signal-to-noise ratio and particle presence. After background and molecular scattering removal, the attenuated backscatter is retrieved assuming nonabsorbing particles. The fully corrected scattering ratio time series are available online from the NDACC data archive.

Temperature and pressure profiles are also available daily from balloon borne radio-soundings operated by Meteo-France since 1957. These soundings are coordinated by WMO and performed at 00:00 UT.

Daily total ozone columns measurements are performed by SAOZ (Système d'Analyse par Observation Zénithale, Pommereau & Goutail, 1988) spectrometer since 1988. The SAOZ is a passive remote-sensing instrument that measures the sunlight scattered from the zenith sky in the visible. Observations are made twice a day during sunrise and sunset allowing total ozone measurements the whole year at the polar circle. Differential Optical Absorption Spectroscopy (DOAS) method is used to retrieve slant ozone columns at twilight. Slant columns are then converted into vertical columns using a daily ozone air mass factor (AMF). The AMF is extracted from look up tables that were calculated by UVSPEC/DISORT radiative transfer model using TOMS version 8 (TV8) ozone and temperature profile climatology. Total ozone columns from SAOZ are part of the NDACC (http://www.ndacc.org). SAOZ performances have been continuously assessed by regular comparisons with other independent observations (e.g., Garane et al., 2019; Hendrick et al., 2011; Koukouli et al., 2015; Van Roozendael et al., 1998). The SAOZ total accuracy, including a 3% cross-section uncertainty, is 6% (Hendrick et al., 2011).

2.3. MERRA-2 Reanalysis: Winds and Geopotential Height

The Modern-Era Retrospective Analysis for Research and Applications, version 2 (MERRA-2) (Gelaro et al., 2017), is the latest atmospheric reanalysis of the modern satellite era produced by NASA's Global Modeling and Assimilation Office (GMAO). In this work, we focus on parameters relevant to SSWs: horizontal u-wind component (zonal wind) and geopotential height.

3. Results

3.1. Temperature Anomalies

To check the date of the beginning of the warming in the stratosphere and follow its progression, we show in Figure 1 (upper panel) the evolution of the IASI temperature profile anomalies in 2019, averaged over the [60–90]°S latitude range, with respect to the average of the past 3 years 2016, 2017, and 2018. Clear signature of the SSW event is seen by IASI that begun on 29–30 August 2019 at altitudes ≥10 hPa and reached a maximum during the period from 19 to 21 September at 15 to 30 hPa (~20 to 24 km). The average increase in stratospheric temperature reached a maximum of 34.4° on 20 September when compared to the past 3 years. We chose to focus on the past 3 years instead of the whole IASI record since the available IASI temperature data record is not homogeneous in time before 2016 (see section 2.1 for more information). Besides, 2015 is associated with a strong ozone depletion event and to low temperatures at the polar cap to which IASI is sensitive. This event is likely linked to a possible intrusion of volcanic plumes from lower latitudes (Ivy et al., 2017).

A recent study by Yamazaki et al. (2020) reports an enhancement from MERRA-2 reanalysis at 90°S and 10 hPa reaching 50.8 K/week. Our IASI data (not shown here) over the same latitude, altitude, and time period show a similar enhancement of 48.8 K/week.

The lower panel of Figure 1 shows the evolution of temperature vertical anomalies during the same period but above the DDU station from radiosonde data (station location is also shown on the figure). The balloon

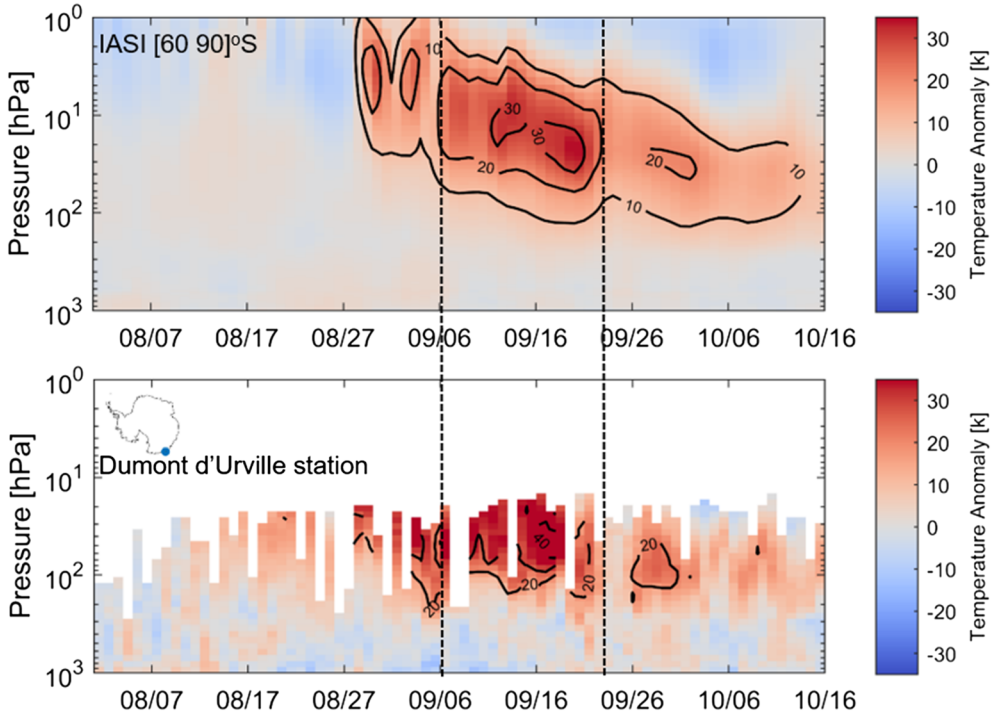

Figure 1. Temperature profile anomalies during the period 1 August to 16 October 2019 with respect to the average of 2016, 2017, and 2018. Upper panel: Temperature anomaly from IASI averaged for latitudes [60–90]°S. Lower panel: Temperature anomaly at the Dumont d'Urville station. Clear signature of the SSW is seen end of August to beginning of September. Dashed lines correspond to the period investigated in Figure 2. Contour lines correspond to 10° change in temperature.

burst-altitude ends the measurements for each radio-sounding (David et al., 2010). Similarly, a clear SSW signature is seen. As compared to the previous 3 years, the ground station measures a temperature increase up to 51° during this SSW event on 18 September and at around 50 hPa. The station records an increase in temperature at a lower altitude, due to its location at the edge of the vortex/outside the vortex, where the mixing of air masses is more important. Moreover, the increase in temperature over the station is higher since temperature anomalies over the station are localized and therefore can be larger than the zonally aggregated IASI data over the whole [60–90]°S latitude range. In fact, Figure 2 hereafter (panels c and d) shows the spatial distribution of the anomaly, and we can see that this average includes regions that are not anomalous.

The time and altitude consistency between the temperature anomalies of the ground based and space borne time series is very good, despite the lower vertical extent of the radiosondes, and the averaging of the satellite data. IASI's temperatures and anomalies at the location of the station are shown in supporting information, Figures S1 and S2. It shows a very good agreement with the temperatures and anomalies recorded at the station.

3.2. Dynamics-Meteorology Interaction

In order to characterize the dynamical interaction with this SSW event, we show in Figure 2 the 18-day average (6–23 September) of the MERRA-2 geopotential height, zonal winds, and temperature anomalies at 10 hPa, with respect to the three previous years. These 18 days correspond to the intensive period of the SSW (between the dashed lines in Figure 1) and are expected to capture the main dynamical features of this SSW event.

During the austral winter, the polar vortex forms over Antarctica. It is generally very stable and concentric with the South Pole terminator. The vortex can also be identified by the coherent region of low geopotential height that is enclosed by the winds. Panel (a) shows the location of the polar vortex as the regions with the

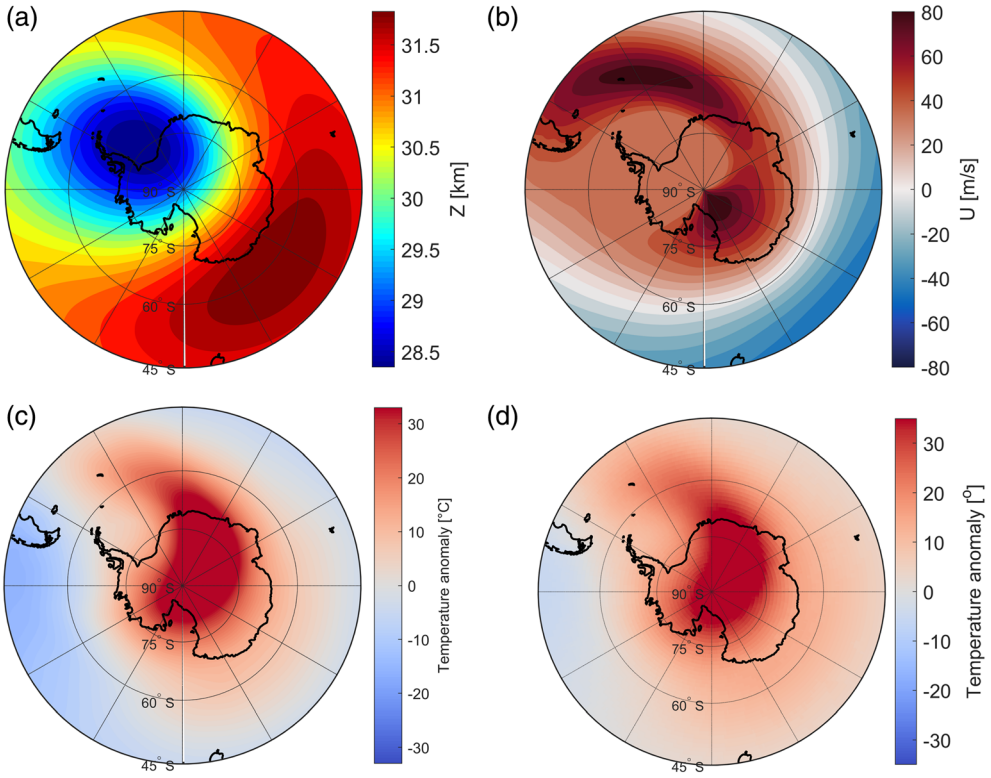

Figure 2. Dynamical and meteorological parameters used to illustrate the SSW event between 6 and 23 September (period between the dashed lines in Figure 1). (a) MERRA-2 geopotential height; (b) MERRA-2 u-wind component at 10 hPa; (c) MERRA-2 temperature anomalies at 10 hPa as compared to the past 3 years; and (d) same as (c) but from IASI.

low geopotential height (low pressure). It is clear that the polar jet is shifted off of its usual center during the 2019 SSW event. In panel (b), a ring of high zonal winds encircles the vortex. The zonal winds do not reverse direction at 60°S everywhere as the polar jet seems to move at latitudes northward 60°S, reaching South America. However, it is worth noting that the zonal winds are anomalous and weakened at 60°S as compared to previous years, due to the vortex weakening. We show in supporting information, Figure S3 that the mean zonal winds during this SSW event period are consistently much weaker than those of previous years. This suggests conditions connected with planetary wave breaking during this SSW event (Yamazaki et al., 2020).

During a standard year, the polar vortex (with the cooler air) is centered over the South Pole. Panels (c) and (d) show the temperature anomalies at 10 hPa from MERRA-2 (panel c) and IASI (panel d). Both are comparable especially that the largest portion of the total number count of observations assimilated in MERRA-2 comes from IASI radiances (Gelaro et al., 2017), so agreement is expected. The temperature anomalies are centered at latitudes southward 75°S, where usually the polar vortex is centered. Moreover, the temperature anomalies show a "tail" of increasing temperature that follows the vortex and the zonal wind pattern highlighting the strong dependence on these parameters on each other.

3.3. Implications on the Ozone and Nitric Acid Total Columns

The polar vortex shape and strength and the variation of temperatures around the vortex in Antarctic winter/spring controls the overall ozone hole size and distribution (Newman et al., 2004). In order to see the uniqueness of this event, we show in Figure 3, upper panel, the IASI ozone total columns anomaly in 2019 with respect to the past 11 years (2008–2018) averaged over 15 September to 15 October of each year. In fact, the ozone hole size was exceptionally small this year as shown in supporting information, Figure S4, where we compare the ozone hole size in 2019 to the mean of 2008–2018 from the Nasa Ozone

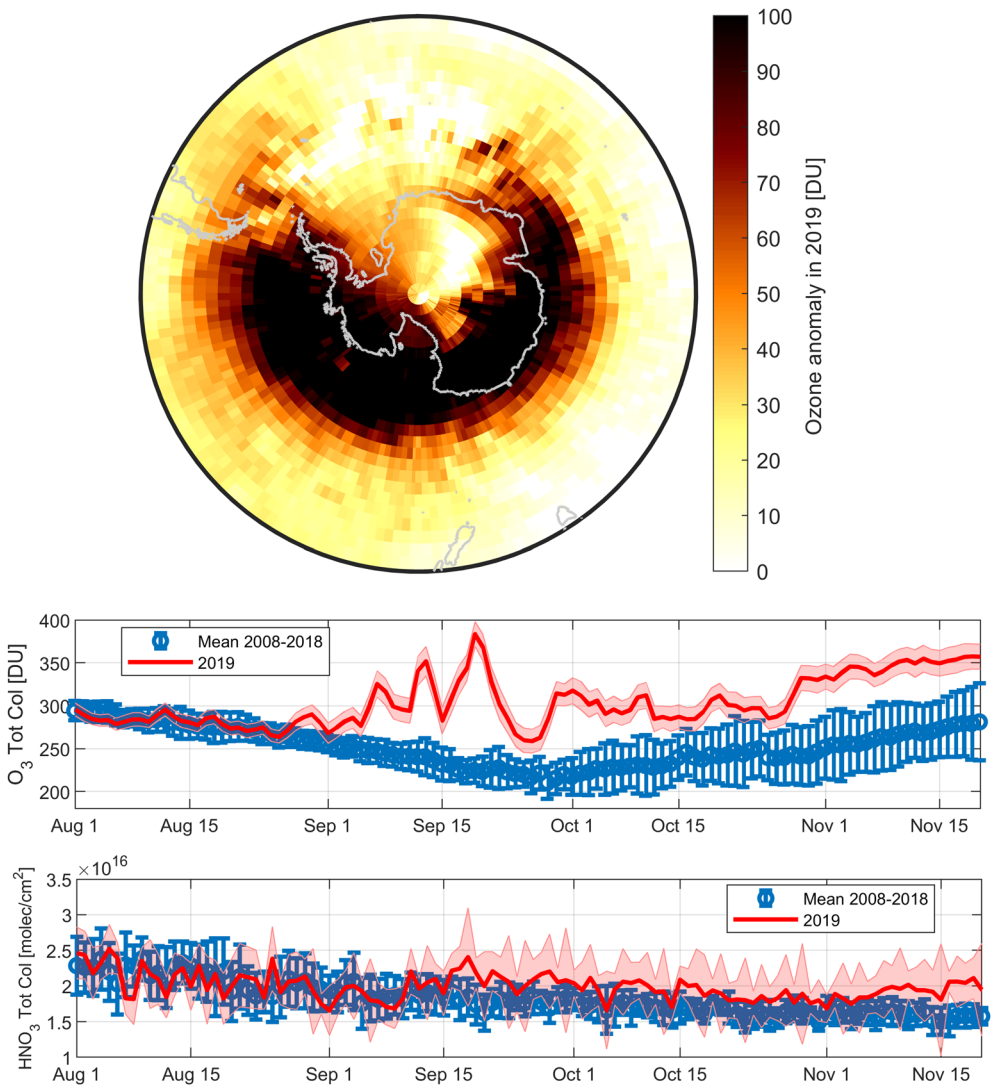

Figure 3. IASI data over the SH (poleward of 45°S from Metop A [2008–2012] and Metop-A + Metop-B [2013–2019]). Upper panel: Ozone total column anomaly in 2019 (2019 − mean$_{[2008–2018]}$) averaged between 15 September and 15 October. Middle panel: Evolution of daily O_3 total columns averaged over the [60–90]°S latitude band for the period 1 August till 20 November of each year. Lower panel: Same as middle panel but for HNO_3. Shaded red areas correspond to errors on the total columns retrieval in 2019, and error bars correspond to the standard deviation around the 11-year mean.

Watch (https://ozonewatch.gsfc.nasa.gov/). Antarctic ozone hole formation typically starts in late August, reaches a maximum in September–October, and starts shrinking afterward (Newman et al., 2004; Scannell et al., 2012—also Figure S4 in supporting information).

The middle and lower panel of Figure 3 shows the daily evolution of O_3 and HNO_3 total columns averaged over [60–90]°S latitude band for September, October, and November. We compare 2019 (in red) with the average of 2008–2018 (in blue). Shaded red curves correspond to the total error associated with the total columns retrieval in 2019 only. They correspond to errors originating from the limited vertical sensitivity, from the measurement noise, and from uncertainties in the fitted (water vapor column) or fixed (e.g., surface emissivity and temperature profile) parameters (Hurtmans et al., 2012). HNO_3 total columnar error is high, ranging between 7% and 40% (in accordance with Ronsmans et al., 2018). This is due to the HNO_3 absorption bands that are weaker and hence the signal-to-noise ratio that is smaller than for O_3, leading to difficulties in the retrieval. Blue error bars represent the standard deviation around the 11-year mean (2008–2018). IASI

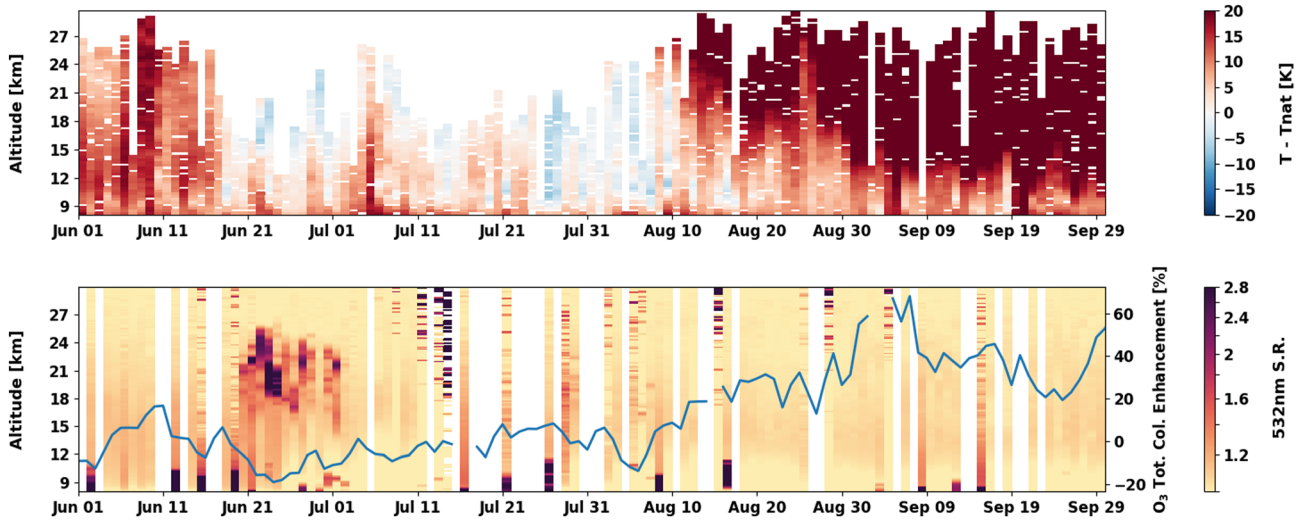

Figure 4. Upper panel: Temperature-NAT formation temperature (T-T_{NAT}) from June to September at Dumont D'Urville. Negative values of T-TNAT are indicative of the likely presence of PSCs. Lower panel: 532-nm attenuated scattering ratio time series from the same time period, as observed by the lidar, superimposed with total ozone columns (blue line, right axis) enhancement with respect to the average of 2008–2018 from the station.

records higher total columns for both species in 2019. Compared to the average of the other 11 years, IASI records in 2019 a sharp increase of 154 DU (Dobson unit) in ozone polar cap total columns on 19 September (69% with respect to other years for both IASIs). For the months of September, October, and November, 2019 was on average higher by 29%, 28%, and 26%, respectively, when compared to the average of the past 11 years, making 2019 the year with highest ozone total columns during this period.

Elevated temperature during this SSW event hindered HNO_3 depletion. The annual cycle of total HNO_3 largely depends on the temperature evolution. Before the austral winter, HNO_3 column increases over the Antarctic and then starts decreasing from June to September because of PSC formation, which has been previously documented by IASI (Ronsmans et al., 2016, 2018) and seen here in Figure 3. HNO_3 total columns record an average increase of 9.7% and 13.9% in September and October, respectively. On 19 September (the day with the highest total ozone column increase), the enhancement is 30%. The increase in ozone and HNO_3 in 2019 is largely due to the changes in the dynamics of the polar vortex generated by the SSW. The early stratospheric warming inside and around the vortex restricted the persistence of PSCs, which is investigated hereafter, leading to lesser activation of halogen species and hence lesser ozone destruction via catalytic reactions, and to lesser denitrification through HNO_3 uptake by PSCs.

PSCs are composed of sulfuric acid (H_2SO_4), nitric acid (HNO_3), and water (H_2O), most often in stacks of relatively fine layers (~1 km) of different physical phase and chemical composition (Dye et al., 1992). As an illustration, the evolution of PSC occurrence from June to September at the DDU station is shown in Figure 4. The 532-nm backscatter ratio is a measure of PSC qualitative occurrence. If the ratio is higher >1, clouds, aerosols, or PSCs are present. Typically, in stratospheric winter, it is used as an indication of PSC presence. The station location is shown in Figure 1. Nitric Acid Trihydrate (NAT) dominated PSC is the most common cloud type observed above DDU (David et al., 2005). NAT formation temperature (T_{NAT}) is calculated from air pressure and climatological mixing ratios of HNO_3 and H_2O (Carslaw et al., 1995).

Stratospheric ozone depletion is related to the persistence of PSC fields, and the overall length of the PSC season is an important indicator to ozone depletion, regulated by temperature evolution. The T-T_{NAT} indicator complements the 2019 lidar time series when no measurements are available, as the instrument is not operated under bad weather conditions.

Profiles where a cirrus layer is present around the tropopause are associated to greater noise at higher altitudes. Overall, the 2019 PSC season is highly unusual at DDU: It started early, around 20 June with very strong PSC layers and high depolarization ratios (not shown here), implying NAT or even possible ice

presence, and the vortex was shifted toward the station with very low temperatures. July and August are typically the months with the strongest PSC episodes, but in the second part of August, the PSC field was shifted along with the polar vortex toward South America (not shown here). The DDU radiosondes suggest that the anomalous warming started at DDU in mid-August, which is also seen in Figure 1 at the station location.

The effect of this altered PSC season on the 2019 O_3 columns at DDU is clear. The collocated SAOZ comparison with the average O_3 of 2008–2018 (blue line—lower panel) shows a clear enhancement. It starts mid-August and reaches a maximum +70% on 8 September. We show in supporting information (Figures S5 and S6) the comparison between IASI-A, IASI-B, and the SAOZ. The figure shows the ozone enhancement averaged monthly at the station location, and IASI-A and IASI-B show good agreement with the SAOZ. As an example, the relative bias in total ozone columns between the SAOZ and IASI averaged for the month of September 2019 was around 1% (supporting information, Figure S6).

4. Conclusions

While SSW events are more common in the NH, we analyze in this study the rare SSW event in the SH that occurred in 2019. We demonstrate the ability of the IASI instruments to detect simultaneously the stratospheric warming and the evolution of the ozone and nitric acid total columns. Dynamics data from MERRA-2 and from the DDU station are used to help in interpreting this event: From the middle to end of August to early September 2019, the polar vortex has been displaced off the pole and weakened by this SSW event. IASI detects an increase in temperatures in the upper stratosphere up to more than 34°C when compared to the average of the past 3 years over the whole [60–90]°S latitude range. Over the same time period, it increased up to 51°C at the DDU station in the low to middle stratosphere, and the polar vortex shape, location, and strength have been affected. The PSC season was halted by the warming, leading to lesser ozone destruction. The ozone total columns reached an increase of 70% on 19 September 2019 when compared to the average of the past 11 years, for both IASI and at the DDU station.

This SSW event is a good illustration of the large variability of the mechanisms governing the ozone loss in the Antarctic stratosphere. The healing of the ozone layer is slow (Wespes et al., 2019), and the return of the springtime total ozone column to 1980 values is expected in 2060s (WMO, 2018). An interesting feature of this event is that it propagated into the surface in late October, unusually delayed (Lim et al., 2020). This aspect was linked to strong positive Indian Ocean Dipole mode (Lim et al., 2020), which will be analyzed by IASI in a future work.

Data Availability Statement

The IASI O_3 and HNO_3 data presented in this paper are publicly available on the AERIS repository (https://iasi.aeris-data.fr/O3 and https://iasi.aeris-data.fr/HNO3; Aeris, 2019). IASI temperature data are available through the EUMETSAT website (eumetsat.int; EUMETSAT, 2019). MERRA-2 data are available through the NASA GMAO website (https://gmao.gsfc.nasa.gov/reanalysis/MERRA-2/) (MERRA-2, 2019). The SAOZ data are available at http://saoz.obs.uvsq.fr (SAOZ, 2019). Dumont d'Urville station data are available at http://www.ndacc.org (DDU, 2019).

Acknowledgments

This work was supported by the CNES. It is based on observations with IASI embarked on Metop. The authors thank Maya George for her help with the review of this manuscript. The authors acknowledge the Aeris data infrastructure for providing access to the IASI data used in this study. The AC SAF project is acknowledged for supporting the IASI FORLI-O3 implementation at EUMETSAT. Operations on the Dumont D'Urville station are supported by the French Polar Institute (Institut Paul-Emile Victor [IPEV]) in the framework of the NDACC Antarctica project. Ground-based instruments are supported by ACTRIS-France and NDACC. The research on IASI is supported in Belgium by Belspo and ESA (Prodex arrangement IASI.Flow).

References

Aeris (2019). The IASI O3 products processed with FORLI-O3, available at: http://iasi.aeris-data.fr/O3/, last access: 12 December 2019.

Andrews, D. G., Holton, J. R., & Leovy, C. B. (1987). *Middle atmosphere dynamics*, (p. 489). San Diego, CA: Academic.

Baldwin, M. (2003). Stratospheric memory and skill of extended-range weather forecasts. *Science*, *301*(5633), 636–640. https://doi.org/10.1126/science.1087143

Baldwin, M. P., & Dunkerton, T. J. (1999). Propagation of the Arctic Oscillation from the stratosphere to the troposphere. *Journal of Geophysical Research*, *104*, 30,937–30,946. https://doi.org/10.1029/1999JD900445

Blume, C., Matthes, K., & Horenko, I. (2012). Supervised learning approaches to classify sudden stratospheric warming events. *Journal of the Atmospheric Sciences*, *69*(6), 1824–1840. https://doi.org/10.1175/JAS-D-11-0194.1

Boynard, A., Hurtmans, D., Garane, K., Goutail, F., Hadji-Lazaro, J., Koukouli, M. E., et al. (2018). Validation of the IASI FORLI/EUMETSAT ozone products using satellite (GOME-2), ground-based (Brewer–Dobson, SAOZ, FTIR) and ozonesonde measurements. *Atmospheric Measurement Techniques*, *11*(9), 5125–5152. https://doi.org/10.5194/amt-11-5125-2018

Butler, A. H., Seidel, D. J., Hardiman, S. C., Butchart, N., Birner, T., & Match, A. (2015). Defining sudden stratospheric warmings. *Bulletin of the American Meteorological Society*, *96*(11), 1913–1928. https://doi.org/10.1175/BAMS-D-13-00173.1

Carslaw, K. S., Luo, B., & Peter, B. (1995). An analytic expression for the composition of aqueous HNO_3-H_2SO_4 stratospheric aerosols including gas phase removal of HNO_3. *Geophysical Research Letters*, *22*(14), 1877–1880. https://doi.org/10.1029/95GL01668

Charlton, A. J., & Polvani, L. M. (2007). A new look at stratospheric sudden warmings. Part I: Climatology and modeling benchmarks. *Journal of Climate*, *20*(3), 449–469. https://doi.org/10.1175/JCLI3996.1

Clerbaux, C., Boynard, A., Clarisse, L., George, M., Hadji-Lazaro, J., Herbin, H., et al. (2009). Monitoring of atmospheric composition using the thermal infrared IASI/MetOp sounder. *Atmospheric Chemistry and Physics*, *9*(16), 6041–6054. https://doi.org/10.5194/acp-9-6041-2009

Cohen, J., Barlow, M., Kushner, P. J., & Saito, K. (2007). Stratosphere–troposphere coupling and links with Eurasian land surface variability. *Journal of Climate*, *20*, 5335–5343. https://doi.org/10.1175/2007JCLI1725.1

David, C., Bekki, S., Berdunov, N., Marchand, M., & Mégie, G. (2005). Classification and scales of Antarctic polar stratospheric clouds using wavelet decomposition. *Journal of Atmospheric and Solar - Terrestrial Physics*, *67*(3), 293–300. https://doi.org/10.1016/j.jastp.2004.07.043

David, C., Bekki, S., Godin, S., & Mégie, G. (1998). Polar stratospheric clouds climatology over Dumont d'Urville between 1989 and 1993 and the influence of volcanic aerosols on their formation. *Journal of Geophysical Research*, *103*(D17), 22,163–22,180. https://doi.org/10.1029/98JD01692

David, C., Haefele, A., Keckhut, P., Marchand, M., Jumelet, J., Leblanc, T., et al. (2012). Evaluation of stratospheric ozone, temperature, and aerosol profiles from the LOANA lidar in Antarctica. *Polar Science*, *6*(3-4), 209–225. https://doi.org/10.1016/j.polar.2012.07.001

David, C., Keckhut, P., Armetta, A., Jumelet, J., Snels, M., Marchand, M., & Bekki, S. (2010). Radiosonde stratospheric temperatures at Dumont d'Urville (Antarctica): Trends and link with polar stratospheric clouds. *Atmospheric Chemistry and Physics*, *10*, 3813–3825. https://doi.org/10.5194/acp-10-3813-2010

DDU (2019). Dumont d'Urville station sonde and lidar data, available at: http://www.ndacc.org, last access: 12 December 2019.

de Laat, A. T. J., & van Weele, M. (2011). The 2010 Antarctic ozone hole: Observed reduction in ozone destruction by minor sudden stratospheric warmings. *Scientific Reports*, *1*, 38. https://doi.org/10.1038/srep00038

Dye, J. E., Baumgardner, D., Gandrud, B. W., Kawa, S. R., Kelly, K. K., Loewenstein, M., et al. (1992). Particle size distributions in Arctic polar stratospheric clouds, growth and freezing of sulfuric acid droplets, and implications for cloud formation. *Journal of Geophysical Research*, *97*(D8), 8015–8034. https://doi.org/10.1029/91JD02740

Eswaraiah, S., Kim, Y. H., Lee, J., Ratnam, M. V., & Rao, S. V. B. (2018). Effect of Southern Hemisphere sudden stratospheric warmings on Antarctica mesospheric tides: First observational study. *Journal of Geophysical Research: Space Physics*, *123*, 2127–2140. https://doi.org/10.1002/2017JA024839

EUMETSAT (2019). IASI level 2—Temperature and humidity profiles—Metop—Regional data service, available at: https://navigator.eumetsat.int/product/EO:EUM:DAT:METOP:EARS-IASI-L2, last access 12 December 2019.

EUMETSAT, IASI Level 2 (2017). Product guide, 11 July 2017, EUM/OPS-EPS/MAN/04/0033, http://www.eumetsat.int/website/wcm/idc/idcplg?IdcService=GET_FILE&dDocName=PDF_DMT_151563&RevisionSelectionMethod=LatestReleased&Rendition=Web.

Garane, K., Koukouli, M.-E., Verhoelst, T., Lerot, C., Heue, K., Fioletov, V., et al. (2019). TROPOMI/S5p total ozone column data: Global ground-based validation and consistency with other satellite missions. *Atmospheric Measurement Techniques European Geosciences Union*, *12*(10), 5263–5287. https://doi.org/10.5194/amt-12-5263-2019-insu-02112717

Gelaro, R., McCarty, W., Suárez, M. J., Todling, R., Molod, A., Takacs, L., et al. (2017). The Modern-Era Retrospective Analysis for Research and Applications, version 2 (MERRA-2). *Journal of Climate*, *30*(14), 5419–5454. https://doi.org/10.1175/JCLI-D-16-0758.1

Hendon, H. H., Thompson, D. W. J., Lim, E.-P., Butler, A. H., Newman, P. A., Coy, L., et al. (2019). Rare forecasted climate event under way in the Southern Hemisphere. *Nature*, *573*(7775), 495–495. https://doi.org/10.1038/d41586-019-02858-0

Hendrick, F., Pommereau, J.-P., Goutail, F., Evans, R. D., Ionov, D., Pazmino, A., et al. (2011). NDACC/SAOZ UV-visible total ozone measurements: Improved retrieval and comparison with correlative ground-based and satellite observations. *Atmospheric Chemistry and Physics*, *11*, 5975–5995. https://doi.org/10.5194/acp-11-5975-2011

Holton, J. R., Haynes, P. H., McIntyre, M. E., Douglass, A. R., Rood, R. B., & Pfister, L. (1995). Stratosphere-troposphere exchange. *Reviews of Geophysics*, *33*(4), 403–439. https://doi.org/10.1029/95RG02097

Hurtmans, D., Coheur, P.-F., Wespes, C., Clarisse, L., Scharf, O., Clerbaux, C., et al. (2012). FORLI radiative transfer and retrieval code for IASI. *Journal of Quantitative Spectroscopy and Radiative*, *113*, 1391–1408. https://doi.org/10.1016/j.jqsrt.2012.02.036

Ivy, D. J., Solomon, S., Kinnison, D., Mills, M. J., Schmidt, A., & Neely, R. R. III (2017). The influence of the Calbuco eruption on the 2015 Antarctic ozone hole in a fully coupled chemistry-climate model. *Geophysical Research Letters*, *44*, 2556–2561. https://doi.org/10.1002/2016GL071925

Kidston, J., Scaife, A. A., Hardiman, S. C., Mitchell, D. M., Butchart, N., Baldwin, M. P., & Gray, L. J. (2015). Stratospheric influence on tropospheric jet streams, storm tracks and surface weather. *Nature Geoscience*, *8*, 433–440. https://doi.org/10.1038/ngeo2424

Klaes, D., Cohen, M., Buhler, Y., Schlüssel, P., Munro, R., Luntama, J.-P., et al. (2007). An introduction to the EUMETSAT Polar system. *Bulletin of the American Meteorological Society*, *88*, 1085–1096. https://doi.org/10.1175/BAMS-88-7-1085

Koukouli, M., Balis, D., Zyrichidou, E., Lerot, C., Van Roozendael, M., Lambert, J. C., et al. (2015). Validating the new GOME/ERS-2, SCIAMACHY/Envisat and GOME-2/MetOp-A homogeneous total ozone climate data record developed as part of the ESA Climate Change Initiative. *Journal of Geophysical Research: Atmospheres*, *120*, 12,296–12,312. https://doi.org/10.1002/2015JD023699

Krüger, K., Naujokat, B., & Labitzke, K. (2005). The unusual midwinter warming in the Southern Hemisphere stratosphere 2002: A comparison to Northern Hemisphere phenomena. *Journal of the Atmospheric Sciences*, *62*, 603–613.

Kuttippurath, J., & Nikulin, G. (2012). A comparative study of the major sudden stratospheric warmings in the Arctic winters 2003/2004–2009/2010. *Atmospheric Chemistry and Physics*, *12*, 8115–8129. https://doi.org/10.5194/acp-12-8115-2012

Lim, E.-P., Hendon, H. H., Butler, A. H., Garreaud, R. D., Polichtchouk, I., Shepherd, T. G., et al. (2020). The 2019 Antarctic sudden stratospheric warming, *SPARC Newsletter*, *54*, 10–13. https://www.sparc-climate.org/wp-content/uploads/sites/5/2017/12/SPARCnewsletter_Jan2020_PRINT.pdf

Lim, E.-P., Hendon, H. H., & Thompson, D. W. J. (2018). Seasonal evolution of stratosphere-troposphere coupling in the Southern Hemisphere and implications for the predictability of surface climate. *Journal of Geophysical Research: Atmospheres*, *123*, 12,002–12,016. https://doi.org/10.1029/2018JD029321

MERRA-2 (2019). The NASA GMAO reanalysis. Retrieved from https://gmao.gsfc.nasa.gov/reanalysis/MERRA-2/, last access 12 December 2019.

Newman, P. A., Kawa, S. R., & Nash, E. R. (2004). On the size of the Antarctic ozone hole. *Geophysical Research Letters*, *31*, L21104. https://doi.org/10.1029/2004GL020596

Pommereau, J.-P., & Goutail, F. (1988). O3 and NO2 ground-based measurements by visible spectrometry during arctic winter and spring 1988. *Geophysical Research Letters*, *15*, 891–894.

Rodgers, C. D. (2000). In N. J. Hackensack (Ed.), *Inverse methods for atmospheric sounding: Theory and practice*, *World Scientific, Series on Atmospheric, Oceanic and Planetary Physics* (Vol. 2). Oxford, UK: World Scientific.

Ronsmans, G., Langerock, B., Wespes, C., Hannigan, J. W., Hase, F., Kerzenmacher, T., et al. (2016). First characterization and validation of FORLI-HNO3 vertical profiles retrieved from IASI/Metop. *Atmospheric Measurement Techniques*, *9*, 4783–4801. https://doi.org/10.5194/amt-9-4783-2016

Ronsmans, G., Wespes, C., Hurtmans, D., Clerbaux, C., & Coheur, P.-F. (2018). Spatio-temporal variations of nitric acid total columns from 9 years of IASI measurements—A driver study. *Atmospheric Chemistry and Physics*, *18*, 4403–4423. https://doi.org/10.5194/acp-18-4403-2018

SAOZ (2019). Total ozone and ozone vertical profile soundings, available at: http://saoz.obs.uvsq.fr, last access: 12 December 2019.

Scannell, C., Hurtmans, D., Boynard, A., Hadji-Lazaro, J., George, M., Delcloo, A., Tuinder, O., Coheur, P.-F., & Clerbaux, C. (2012). Antarctic ozone hole as observed by IASI/MetOp for 2008–2010. *Atmospheric Measurement Techniques*, *5*, 123–139. https://doi.org/10.5194/amt-5-123-2012

Scherhag, R. (1952). Die explosionsartige Stratospharenerwarmug des Spatwinters 1951/52. *Berlin Deutsche Wetterdieustes*, *6*, 51–63.

Solomon, S. (1999). Stratospheric ozone depletion: A review of concepts and history. *Reviews of Geophysics*, *37*, 275–316. https://doi.org/10.1029/1999RG900008

Solomon, S., Garcia, R. R., Rowland, F. S., & Wuebbles, D. J. (1986). On the depletion of Antarctic ozone. *Nature*, *321*, 755–758. https://doi.org/10.1038/321755a0

Van Damme, M., Whitburn, S., Clarisse, L., Clerbaux, C., Hurtmans, D., & Coheur, P.-F. (2017). Version 2 of the IASI NH3 neural network retrieval algorithm: Near-real-time and reanalysed datasets. *Atmospheric Measurement Techniques*, *10*, 4905–4914. https://doi.org/10.5194/amt-10-4905-2017

Van Roozendael, M., Peeters, P., Roscoe, H. K., de Backer, H., Jones, A. E., Bartlett, L., et al. (1998). Validation of ground-based visible measurements of total ozone by comparison with Dobson and Brewer spectrophotometers. *Journal of Atmospheric Chemistry*, *29*(1), 55–83. https://doi.org/10.1023/A:1005815902581

Varotsos, C. (2003). What is the lesson from the unprecedented event over Antarctica in 2002? *Environmental Science and Pollution Research*, *10*(2), 80–81. https://doi.org/10.1007/BF02980093

Wang, Y., Shulga, V., Milinevsky, G., Patoka, A., Evtushevsky, O., Klekociuk, A., et al. (2019). Winter 2018 major sudden stratospheric warming impact on midlatitude mesosphere from microwave radiometer measurements. *Atmospheric Chemistry and Physics*, *19*(15), 10,303–10,317. https://doi.org/10.5194/acp-19-10303-2019

Wespes, C., Hurtmans, D., Chabrillat, S., Ronsmans, G., Clerbaux, C., & Coheur, P.-F. (2019). Is the recovery of stratospheric O3 speeding up in the Southern Hemisphere? An evaluation from the first IASI decadal record (2008–2017). *Atmospheric Chemistry and Physics*, *19*, 14,031–14,056. https://doi.org/10.5194/acp-19-14031-2019

WMO (1978). WMO Commission for Atmospheric Sciences, Abridged Final Report of the Seventh Session, Manila, 27 February-10 March 1978. WMO No. 509. (p. 36, item 9.4.4).

WMO (2002). Antarctic ozone hole splits in two. Press Release No. 681, October 1, 2002.

WMO (2018). Scientific assessment of ozone depletion: 2018, Global Ozone Research and Monitoring Project–Report No. 58, 588 pp., Geneva, Switzerland.

Yamazaki, Y., Matthias, V., Miyoshi, Y., Stolle, C., Siddiqui, T., Kervalishvili, G., et al. (2020). September 2019 Antarctic sudden stratospheric warming: Quasi-6-day wave burst and ionospheric effects. *Geophysical Research Letters*, *47*, e2019GL086577. https://doi.org/10.1029/2019GL086577